

TECHNOLOGY DEVELOPMENT FOR EXOPLANET MISSIONS

Final Technology Milestone Report
NASA Grant No. NNX12AD98G

JPL Document D-93599

VERIFYING DEPLOYMENT TOLERANCES OF AN EXTERNAL OCCULTER FOR STARLIGHT SUPPRESSION

PROF. N. JEREMY KASDIN
PRINCIPAL INVESTIGATOR
PRINCETON UNIVERSITY
MECHANICAL AND AEROSPACE ENGINEERING

June, 2014

CoInvestigators:

David N. Spergel (Science PI), Robert Vanderbei, Princeton University; Stuart Shaklan (Institutional PI), Doug Lisman, Mark Thomson, Jet Propulsion Laboratory, California Institute of Technology; Geoff Marks, Amy Lo, Northrop Grumman Aerospace Systems; Bruce Macintosh, Lawrence Livermore National Laboratory.

Other Key Personnel:

Eric Cady, David Webb, Jet Propulsion Laboratory

Approvals

Released by:



06/30/14

N. Jeremy Kasdin
Principal Investigator, Princeton University

Approved by:



08/21/14

Peter R. Lawson
Exoplanet Exploration Program Chief Technologist, JPL



8/21/14

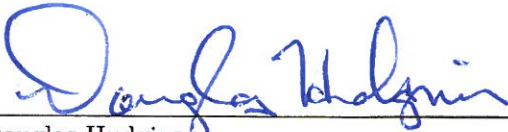
Nicholas Siegler
Exoplanet Exploration Technology Manager, JPL



8/25/14

p.p.

Gary Blackwood
Exoplanet Exploration Program Manager, JPL



8/26/2014

Douglas Hudgins
Exoplanet Exploration Program Scientist, NASA HQ



9/2/2014

John Gagosian
Exoplanet Exploration Program Executive, NASA HQ

CONTENTS

1. Executive Summary	4
2. Certification	4
3. Success Criteria	5
4. Occulter Design Summary	5
5. Experiment Design	6
5.1. Hub Design and Manufacture	6
5.2. Petal Design and Manufacture	6
5.3. Petal-Truss Interface Design and Manufacture	7
5.4. Truss Spokes	9
6. Deployments and Metrology	9
6.1. Initial Shimming and Metrology	9
6.2. Partial Deployments	11
7. Processing and Analysis	11
7.1. Data collection	11
7.2. Data processing	13
7.3. Analysis and application to milestone	15
8. Conclusions	18
9. Acknowledgement	20
Appendix A. Success Criteria from White Paper	21
Appendix B. Table of Acronyms	22
References	23

1. EXECUTIVE SUMMARY

In this final report, we document the results of our ROSES Technology Development for Exoplanet Missions (TDEM) two-year research program to advance the technology associated with external occulter deployment. Following our first successful TDEM on occulter petal manufacturing, in this TDEM we addressed the next “tall technology pole” of precision deployment. To that end, we manufactured four sub-scale petals and a custom hub. We attached the petals to an existing deployable truss which itself was attached to the hub. Using a gravity offloading fixture we deployed the truss with attached petals fifteen times and used precision metrology to demonstrate that we met the required accuracy. We described the occulter optical and mechanical design, the truss and hub design and development, and the error analysis as well as the goals of the program in our Technology Milestone Whitepaper, JPL Document D-81165 dated October, 2013. We will refer to that often in this report.

We show in this report that a our petal mechanical design can be integrated onto a deployable truss and hub and deployed to the required accuracy described in our whitepaper consistent with an error analysis that results in an external occulter achieving our targeted contrast ratio development goal.

As a reference, our milestone from the whitepaper is:

TDEM Occulter Milestone:

- Verify that the deviations of the petal base point from the design circle are repeatedly below the 3σ positioning requirement for a 10^{-9} contrast using a sufficient number of deployments to verify the requirements are met with 90% confidence.

In the remainder of this report we present the results that demonstrate we met the milestone with substantial margin. The whitepaper describes the error analysis showing that for this subscale occulter and relaxed contrast of 10^{-9} , the required deployment accuracy, both lateral and radial, is ± 0.95 mm. Unfortunately, in the whitepaper we mistakenly scaled both the lateral and radial requirements for occulter size when in fact only the radial scales, making the lateral requirement for 10^{-9} contrast 1.6 mm. We achieved these deployment accuracies with better than 90% confidence over 15 partial stow and deploy cycles (after 5 initial full stow and deploys followed by shimming). In fact, the deployments so exceeded the milestone that when scaled to a full size occulter the corresponding contribution to contrast is better than 10^{-12} , almost an order of magnitude better than the error budget for a flight system.

2. CERTIFICATION

In this section, we reference the list of items for the certification data package from Section 6 of the milestone whitepaper and identify where they can be found in this report. The certification item description from the whitepaper is given in italics followed by the reference information in roman type.

- (1) *A narrative report, including a discussion of how each element of the milestone was met, and a narrative summary of the overall milestone achievement.*
This narrative report responds to item (1) of the certification data package.
- (2) *Description of truss, hub and petal designs and materials and assembly steps.*
See Section 5.
- (3) *Description of the photogrammetry metrology system and certification.*
See Section 6.
- (4) *Description of the metrology process.*
See Section 6 and Section 7.1.

- (5) *Description of the model fitting and data analysis process and results including error estimates and best fit circle biases.*
See Section 7.2.
- (6) *Description of the milestone determination and certification.*
See Section 7.3.

3. SUCCESS CRITERIA

Appendix A reproduces verbatim the success criteria from the milestone whitepaper. Here we reference those criteria and indicate where in this report evidence of success or a description of the process can be found.

- (1) The petals were successfully manufactured, installed on the truss, stowed, and deployed using the gravity offload fixture. A description of the hub design and manufacture can be found in § 5.1, the petal design and manufacture in § 5.2, and the petal-truss interface in § 5.3. A picture of the petals after unfurling can be found in Fig. 9.
- (2) The truss was successfully deployed multiple times with the attached petals. A description of the initial deployments and shimming can be found in § 6.1. A description of the full and partial deployments is given in § 6.2.
- (3) A description of the metrology system used to measure the petal base points is given in § 6. A picture of the deployed truss and petals with the laser tracker targets can be found in Fig. 7.
- (4-5) The process for performing the fit to the design circle and for determining the radial and transverse displacement of each base point is given in § 7.2.
- (6) Because of the use of partial stows we were able to perform many more cycles than described in the whitepaper (15 rather than 5). The processing of the 15 data sets to determine the best estimates of the radial and transverse displacements with confidence intervals is described in § 7.3. The milestone was met with better than 90% confidence.

4. OCCULTER DESIGN SUMMARY

The technology whitepaper for this TDEM provides background on occulters for exoplanet imaging; we will not repeat it here for brevity. Our approach to designing occulters uses optimization tools to determine the apodization that results in the smallest and closest possible occulter while still achieving the starlight suppression requirement over a desired wide spectral band.⁽¹⁾ This makes it easier to manufacture and handle, reduces the size of the launch vehicle and fairing, and increases the potential science yield. Hence, the requirements we describe in the whitepaper and here are the tightest possible, specifying the allocated contrast at the smallest inner working angle (IWA) of the smallest possible occulter. (Making larger occulters for the same science objectives results in relaxed tolerances.) For this TDEM we modified the occulter design slightly from our first TDEM (where the occulter was designed for a 1.5 m telescope¹). Because of the smaller size of the available truss, we re-optimized the petals to meet the contrast requirement for the subscale starshade.

Our milestone whitepaper also describes the error budgeting and tolerancing process. For a flight system employing a 32 m starshade with 20 m truss, the requirements on the radial and lateral displacement standard deviation of a petal are ± 0.5 mm 3σ with a radial bias requirement across all petals of less than 0.25 mm 3σ (there is no global requirement on the lateral bias due to the circular symmetry). These correspond to the allocated contrast of 2.2×10^{-11} (for a flight contrast of 10^{-10}) to deployment errors described in the whitepaper. These values were then scaled to account for the sub-scale star shade size and the relaxed contrast of 10^{-9} . Unfortunately, in the

¹Note that there is a typo in Table 1 of the whitepaper; the second column should be labeled a 32 m starshade, not a 23 m starshade.

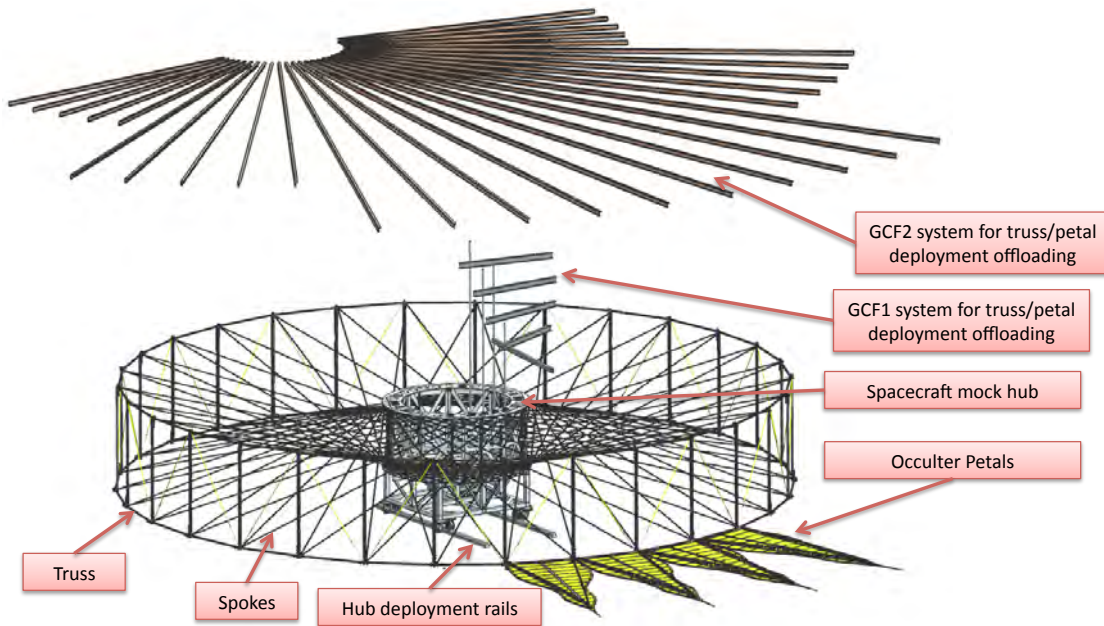


FIGURE 1. Occluder deployment test system with gravity offload fixture.

whitepaper we mistakenly scaled both radial and lateral for the smaller starshade when only the radial requirement should be scaled. The correct scaled requirements for the 12 meter truss and a 10^{-9} contrast become ± 0.95 mm radial standard deviation, < 0.1 mm bias and ± 1.6 mm lateral.

5. EXPERIMENT DESIGN

Figure 1 shows a drawing of the experimental setup consisting of a central hub, a deployable truss, the truss-to-petal interfaces and the starshade petals along with a schematic of the gravity offload fixture. The design and manufacture of these subsystems is described in the following subsections.

5.1. Hub Design and Manufacture. The central hub shown in Figure 1 and Figure 2 provides a stiff body, emulative of the condition we will have in flight from which to deploy the truss and petals. The hub was designed by Northrup Grumman Aerospace Systems (NGAS), Carpinteria, with high level requirements from JPL. The design allows 120 truss spokes to attach tangentially from the two parallel discs at the top and bottom of the hub to the individual nodes of the truss. This bicycle wheel spoke design, from central hub to truss, creates a stiff structure to which we attached our starshade petals. The hub was designed to have interfaces for features that allow the truss to collapse and stow around its outer perimeter. The petals then furl around the truss/hub system and mount against mounting hardware that protrudes from the hub and through the truss. Additional gravity compensation fixture hardware (GCF1) designed by JPL, offloads the weight of the petals during the unfurling stage of the deployment. The central hub, hub deployment rails and petal attachment points were fabricated by NGAS.

5.2. Petal Design and Manufacture. A critical component of the deployment positioning and repeatability requirement, the starshade petals were constructed in the summer of 2012 over a ten week period by two Princeton and two MIT undergraduate summer students. The starshade petals consist of a center spine, or backbone, a base spine to interface to the truss and structural edges to which the optical edges attach. The structural edges are tied back to the center spine via the battens and the whole structure is given shear stiffness from the longerons. In order for the

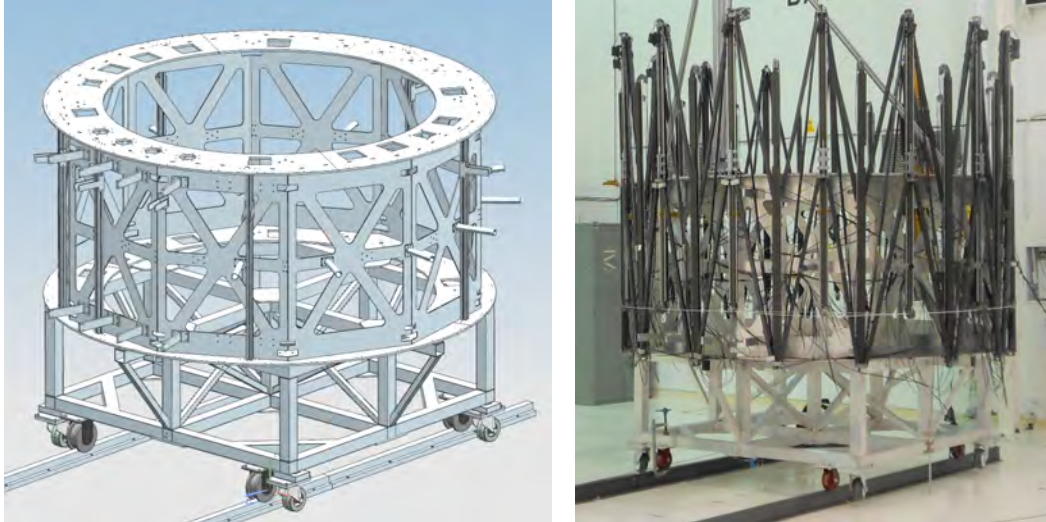


FIGURE 2. As-Built Hub at NGAS Goleta Facility

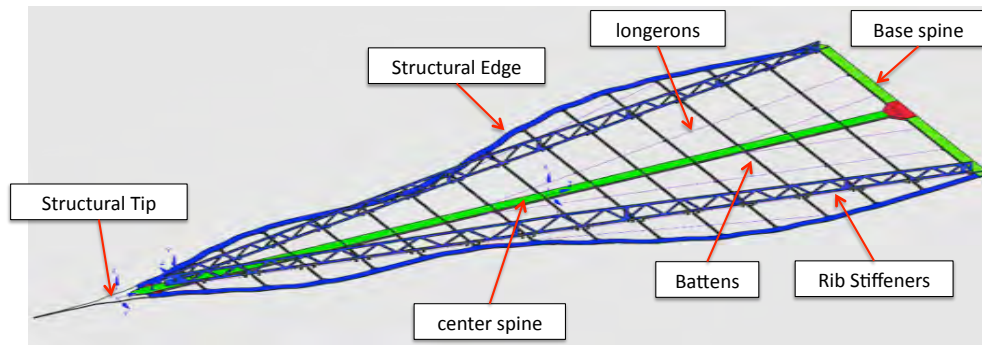


FIGURE 3. Occulter Petal Design

entire petal to wrap around the spacecraft, a flexible material was used as the core of the petal center spine. This unique design allows for the petal to be flexible enough to furl around a 3 meter spacecraft hub and also passively become rigid as the petal unfurls and a pair of spring loaded ribs deploy and rigidize the petal. A schematic of the petal design (the same is in our first TDEM) is shown in Figure 3 and the completed as-built petals are shown in Figure 4 attached to a wooden mock-up of the hub before shipment to NGAS.

5.3. Petal-Truss Interface Design and Manufacture. The petals mount to the truss longerons with precision pinned tabs and clevis joints. The deployment tolerance milestone applies to the petal attachment points and more specifically, the center of each interface joint. This center point was precisely characterized relative to petal mounted targets using photogrammetry. Figure 5 shows the partially stowed truss attached to the hub with the petals attached to the longerons ready for deployment.

The design of the existing Northrup Grumman truss was not commensurate with a petal to longeron interface that would allow furling of the petals around the truss in the stowed condition. For this reason, the fittings that were used to attach the petals to the truss were designed to meet the requirement of quick and repeatable detachment of the petal from the truss longerons via a quick release style fitting that was also designed to maintain the position of the petals with respect to the truss with great precision. Also designed into the petal-to-truss interface fitting is



FIGURE 4. As-Built Petals on Mock Hub

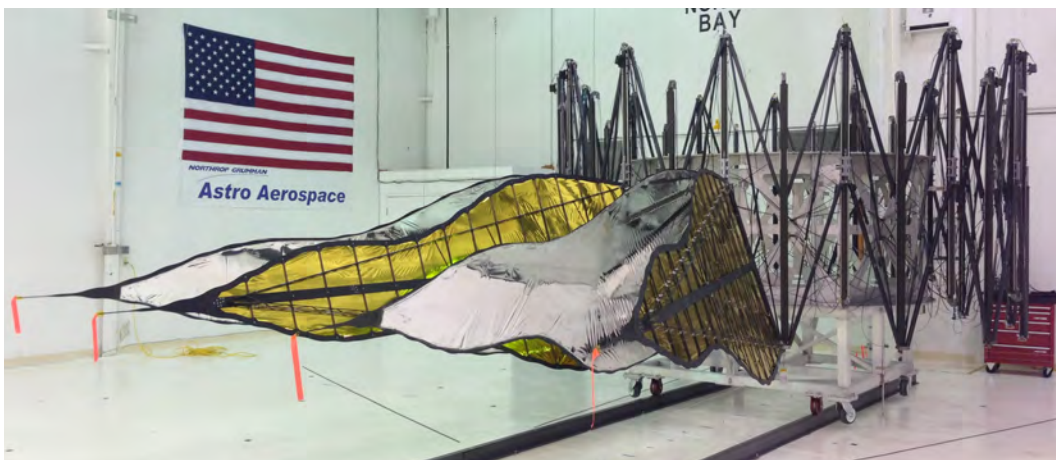


FIGURE 5. As-built petals attached to partially stowed truss.

the ability to shim the petal in the truss radial direction, allowing us to correct for absolute radial position error of the petals after our first set of measurements. The interface fitting consists of two pieces, one that is permanently attached to the truss and the other that is attached to the petal via the quick release mechanism already mentioned. Repeatability of the petal position pre- to post-shimming was maintained via registration features between the two parts of the fitting; this allowed repeatability over an order of magnitude better than our requirement.

Placing the petal interface fittings with the required precision to meet the milestone required a tool that would repeatedly place each petals interface fittings with respect to known locations on the truss. The tool that was used to place the petal-to-truss interface fittings was a single piece and was the same tool that was used for placing the petal interfaces into the petal base spine to which the petal-truss fitting connect.

Placement of the petals with respect to known locations on the truss requires a truss that has known and repeated features at each bay of the truss to which the petal placement tool can be referenced. In our case this was a challenge as the truss was not designed with any known and repeated features to which we could reference and only every other node of the truss was identical. An additional challenge was that the truss model available to us was later found to vary from the as-built prototype. Because only every other node of the truss was identical, this created mirror image bay pairs to which we were only able to reliably place pairs of petals that were symmetric about the node that contained the reliable feature to which we could reference. This node that

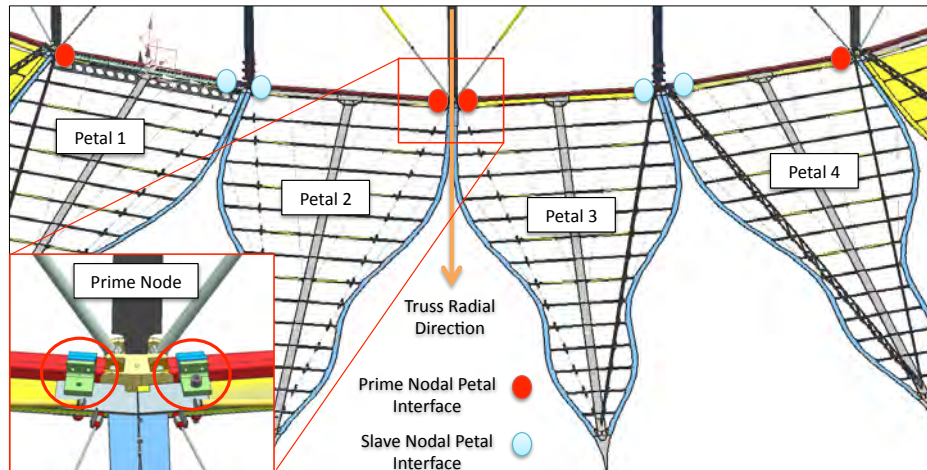


FIGURE 6. Relative tangential relationship of petals. Dots represent the petal interfaces and the colors indicate whether the interface is attached to a prime or dependent node.

contained reliable features is referred to as the prime node, which in our case was centered on the inner two of the four petals. The node that was not referenced for tangential positioning of the petals is referred to as the slave node. Because of this, the two outer petals referenced prime nodes that were the second node removed from the reference point of the two inner petals. This meant that the two outer petals could not be well related tangentially to the two inner petals. This relationship can be seen in Figure 6.

5.4. Truss Spokes. With the given position repeatability requirements for the petal root points, it was critical to create a very stiff connection from the petal roots back to the very stiff central hub structure. This was accomplished via a very stiff spoke that connected the nodes of the truss, to which the petal roots were very well coupled, and that was flexible when not tensioned so as to allow for easy stowing. The stiffness and thus repeatability of the system was achieved by choosing a material that was very low strain, thus reducing deflection and increasing repeatability. These spokes were also very thermally stable, which in our case was important not only for flight but also for testing, due to the very high precision required for the petal root positions.

A challenge encountered in using these spokes was managing the long lengths of each of the 120 spokes during truss deployment such that the spokes would not catch on any of the truss or hub features and break. This was very important in that even one broken spoke could be responsible for changing the overall position of the petals. This required designing a spoke deployment method that controlled the spokes during deployment such that incremental lengths of the spokes were released as the truss deployed. This was accomplished with numerous small spring-like restraints that constrained the length of the spoke. Lower restraint springs were used on the length of the spring near the truss connection and increasing resistance was used as the spoke approached the hub. This resulted in a very robust spoke deployment system that constrained incremental lengths of the spokes to release from their restraints only as the deploying truss tugged them out of their restraints.

6. DEPLOYMENTS AND METROLOGY

6.1. Initial Shimming and Metrology. The initial metrology plan called (described in the milestone whitepaper) for the use of photogrammetry to measure absolute positions at the roots of the petals as well as a number of points spread over each petal and the entire truss. With

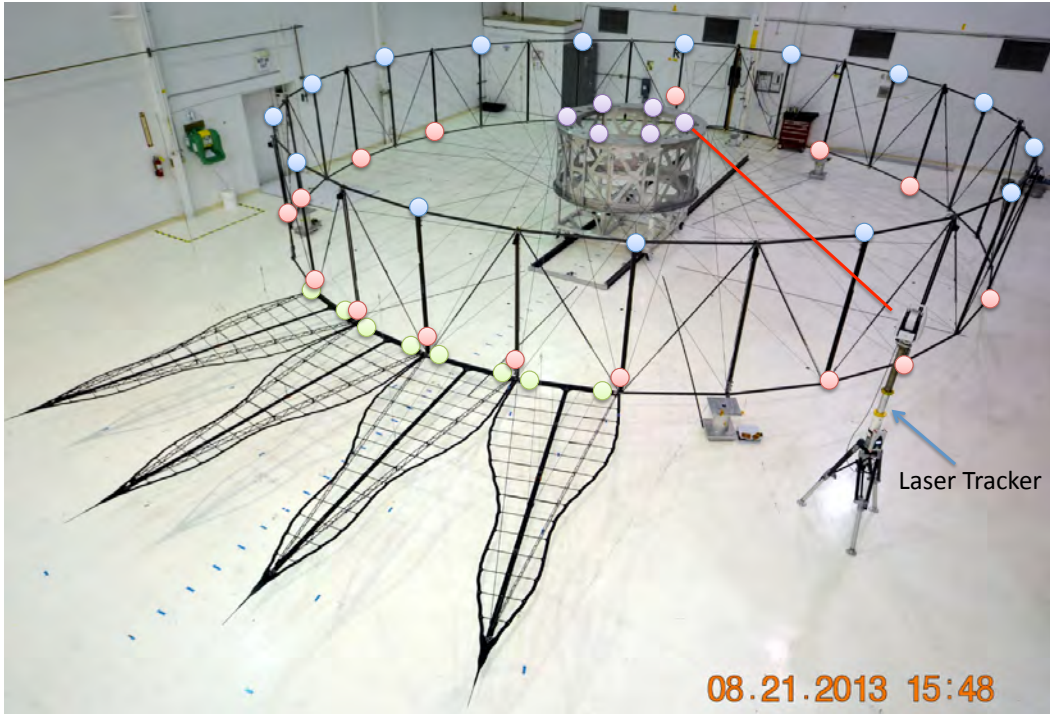


FIGURE 7. Laser tracker and corner cube locations shown on fully deployed system.

many points all over the truss and petals, this would give us many data points to determine the repeatability of the truss deployment. Additionally, a laser tracker, referenced to a few points, was also used for comparison, though the number of corner cubes applied was relatively small compared to the number of photogrammetry targets placed all over the truss, hub, and petals. We in fact used both for the initial estimates of the petal positioning before shimming. After completing pre-shim data analysis, however, it was found that the precision of the photogrammetry system was strongly dependent on target position on the occulter, a fact attributed to the geometry of the bay used for the deployment. The pre-shim data analysis measurements showed that the laser was able to provide more accurate results for our specific location as photogrammetry requires large angle triangulation, which was not available in our space constrained test area. Moreover, the precision of the laser tracker was uniformly better than the photogrammetry system

Once it was determined that the laser tracker was more accurate, the laser tracker was used for the shim installation, post-shim data collection, and to measure the 8 petal root points as well as 42 other points on the truss nodes during deployment. Verification of the accuracy of each laser tracker measurement was performed by measuring each of the 50 points sequentially a total of three times and then comparing these measurements. If one measurement read an error, that measurement was compared to the other two measurements from the same deployment, and if those were in agreement and the initial erroneous, the erroneous measurement was removed. The laser tracker setup with respect to the starshade system can be seen on the fully deployed system in Figure 7.

To shim the petals, a fit was performed to a set of model points using the procedures outlined later in Section 7.2. The differences, all less than 0.25 mm, were taken out manually in the radial direction with known shim increments at the petal-to-truss interface fitting (The architecture did not allow shimming in the tangential direction.) This proved effective; a post-shim measurement showed that the mean offset from the model in the radial direction decreased from 0.151mm to

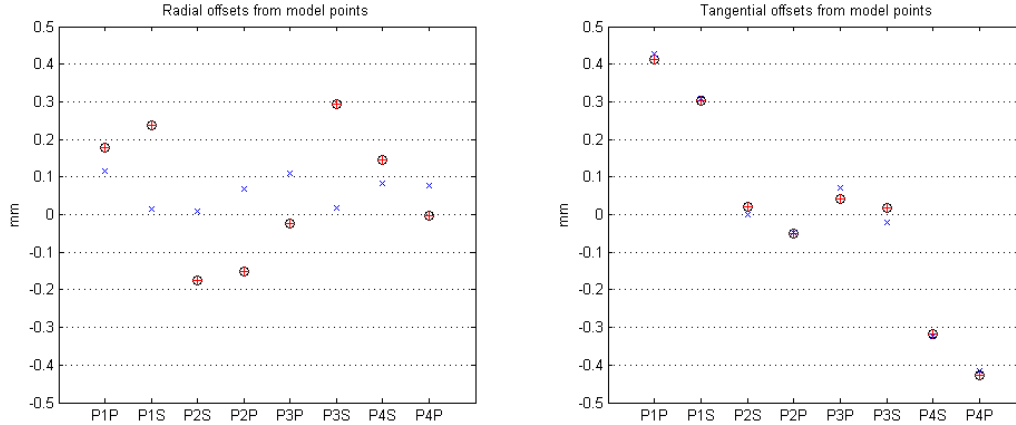


FIGURE 8. Offsets between data and model points before and after shimming. Pre-shim points are designated with black circles with red crosses and post-shim points with blue Xs. *Left.* Radial direction (shimmed) *Right.* Tangential direction (not shimmed)

0.063mm. The tangential direction remained virtually unaltered as expected, with a mean difference of 0.016mm between before- and after-shim model offsets. Figure 8 shows both of these cases.

6.2. Partial Deployments. Initial plans called for furling the petals around the stowed truss between some of the deployments. However, because the gravity compensation system for furling the petals around the truss required a large structure mounted to the top of the hub that contained swinging rails that would rotate across the truss deployment path, it was determined that mounting this hardware to the hub before taking deployment data posed several risks. First it was possible to damage the truss while mounting the hardware on top of the hub, a procedure that could only be performed after the hub was inside the truss structure. Additionally, there was a concern that detaching all the necessary truss gravity offloader lines would be extremely time consuming, posing a risk to achieving the number of deployments required to achieve 90% confidence. Additionally, upon reviewing the petal interface to the truss, it was determined that petal furling would not contribute to any change in the petal root position points that were being measured, as the base spines were registered to stiff fittings that were firmly inserted into petal base spine and thus would not be affected by furling. Another reason for furling the petals would be to determine the effect of petal furling on the truss longerons. Because the existing truss design did not allow us to leave the petals attached to the truss longerons for stowing, but rather we had to detach the petals completely from the truss, the petals could not impart loads on the longerons during furling. For these reasons, no measurable gain would be realized in furling the petals between deployments. The petal unfurling gravity offloader hardware can be seen in Figure 9.

7. PROCESSING AND ANALYSIS

The final tests occurred in October, 2013 at the Northrop Grumman Aerospace Systems (NGAS) Astromesh production facility in Goleta, CA. Based on the 10 deployments with metrology performed in August 2013 to determine petal shimming amounts, 15 partial stow and deploy cycles were completed in October to verify the milestone. Fig. 10 shows a picture of the fully deployed truss with petals attached.

7.1. Data collection. The final set of data consists of 16 deployments: an initial re-deployment following the installation of the radial shims, and 15 stow-and-deploy cycles on the same day as the

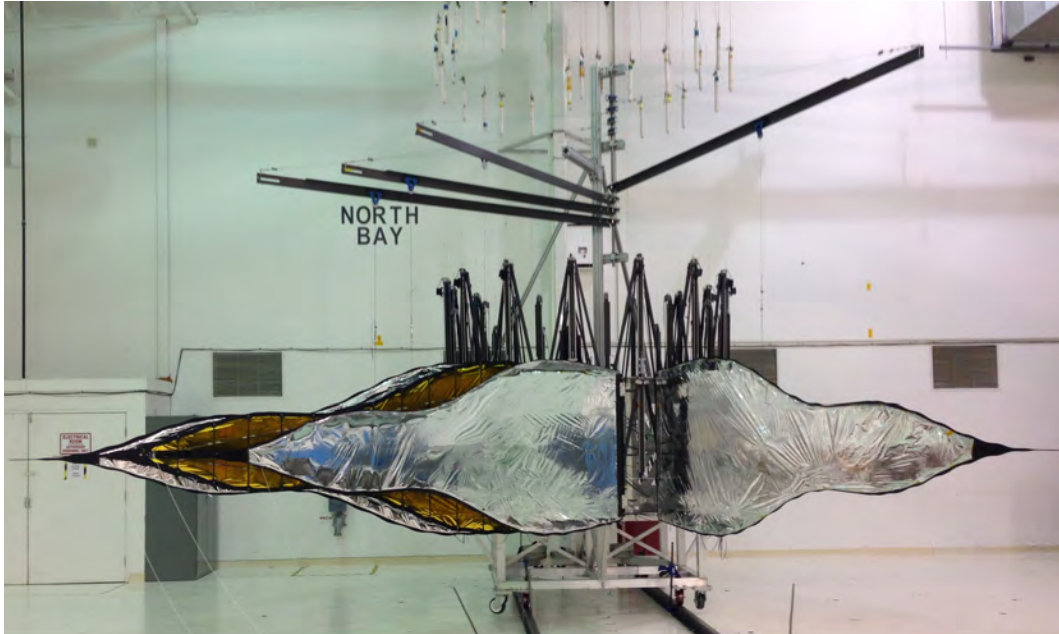


FIGURE 9. Unfurled petals with gravity offloading fixture.



FIGURE 10. The fully deployed truss with attached petals.

initial re-deployment and the two subsequent days. These cycles were a mixture of 10 10%-stows and 5 50%-stows, with the stow percentage representing roughly the fraction of the total radial motion of the truss which was exercised.

During the initial photogrammetry tests, 7 20%-stows were taken along with 3 100%-stows. The mean locations of the petal root points were examined for both the partial- and full-stow cases, and the residual differences in the locations of the resulting data points, shown in Figure 11, were found to be of comparable order to the $75\mu\text{m}$ position-error specification for the V-STARS

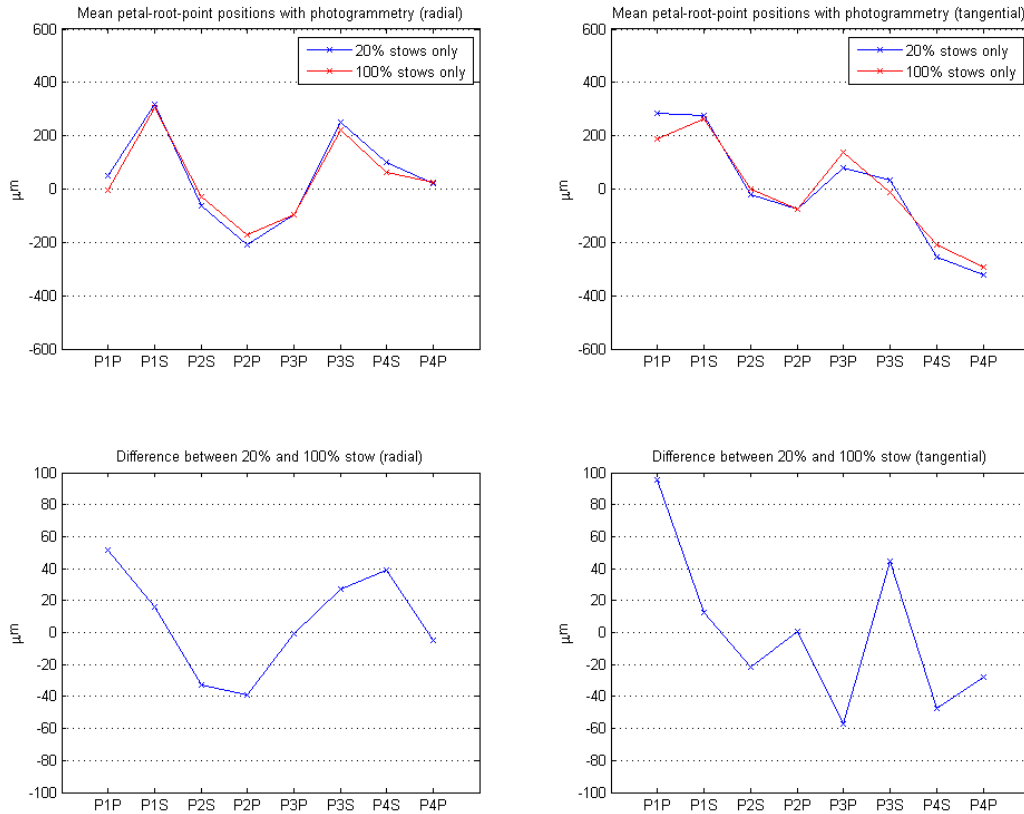


FIGURE 11. *Top.* Mean locations for the petal root points with partial stows (20% stowed) and full stows (100% stowed), in radial and tangential directions. *Bottom.* Differences between the partial- and full-stow cases. Unlike the data in the rest of the figures in this report, this data was taken with a photogrammetry system rather than a laser tracker. With the exception of the P1P point in the tangential direction, all differences are within the $\pm 75\mu\text{m}$ error bars of the photogrammetry system.

system. Given the longer periods of time required for the full stow—3 hours or more, compared to 30 minutes for a 50%-stow and 10 minutes for a 10%-stow—we decided to use a mixture of partial stows only in the post-shim testing. A listing of the data sets is given in Table 1.

7.2. Data processing. Each data set consists of three subsets which were taken in immediate succession without moving the deployed occulter. We expect, since the occulter was not moved between the three 45-second-long data collections, that these points should be identical except for the small random measurement error of the laser tracker, and for the most part this is true. However, there are occasionally strong outliers in a single data point from one of the three sets, which introduce nontrivial deviations in the locations of the measured points if the means of the three subsets are used. To avoid these deviations—which given the correspondence between the measured positions in the other two subsets, we believe to be nonphysical—we instead use the median of the three subsets as the canonical data value for that set.

TABLE 1. Deployments with laser tracker

Date	Designation	Type
10/29/13	BASELINE	-
10/29/13	DEPLOY1	10%-stow
10/29/13	DEPLOY2	10%-stow
10/29/13	DEPLOY3	10%-stow
10/30/13	DEPLOY4	10%-stow
10/30/13	DEPLOY5	10%-stow
10/30/13	DEPLOY6	10%-stow
10/30/13	DEPLOY7	10%-stow
10/30/13	DEPLOY8	10%-stow
10/30/13	DEPLOY9	10%-stow
10/30/13	DEPLOY10	10%-stow
10/30/13	DEPLOY11	50%-stow
10/31/13	DEPLOY12	50%-stow
10/31/13	DEPLOY13	50%-stow
10/31/13	DEPLOY14	50%-stow
10/31/13	DEPLOY15	50%-stow

To co-fit the separate deployments, all 16 deployment datasets are placed into a single nonlinear least-square fit, which translates and rotates each of the 16 sets of data as a rigid body to co-align them. (As it is unreferenced to external fixed points, the resulting coordinate system is only unique up to a constant global translation and rotation, but this gauge transformation does not affect our analysis.) Not all of the data points are used for this fit, however. The rigid structure of the hub is not perfectly coupled to the truss, and neither are the petal tips. We exclude these points from the truss-coalignment fit, though we do apply the resulting coordinate transforms to look at the spreads of hub and petal-tip points.

Three points were excluded from the analysis altogether on physical bases:

- Point PT1, the tip of petal 1, is excluded from all analysis, as the corner cube being used to locate that point fell off halfway through the testing, and could not be put back in exactly the same location.
- One of the strings in the gravity offloader was found to lie exactly between the laser tracker and point OTR14, one of the points on the truss ring on the opposite side from the plane containing the petals. (See Figure 12.) The measured location of this point thus turned out to be extremely unreliable, and was excluded.
- Point PTR13, a point on the same ring of the truss as the petals, was only intermittently visible to the laser tracker camera. It was missed more often than not and thus was excluded from fits.

Conversely, no other point (hub and petals included) was excepted from further analysis. Data quality was not used as a metric for excluding points; while some points appear suspect based on the data spread (e.g. HUB2, PTR8), we do not exclude them without a corresponding physical explanation for their excision.

After the deployments are aligned to each other, we extract the points located at nodes at the root of each petal. These nodes are also present in a CAD model of the system, falling on a circle, and the locations of these nodes in the model were also extracted; the two were then fit against each other to determine the correspondence between measured and model points.

The milestone specification called for a fit to a best-fit circle rather than points extracted from a structural model of the system. However, using explicit points in a model in the fit provides two primary advantages:

- (1) Using points derived from a model provides traceability between desired and measured locations for the nodes.

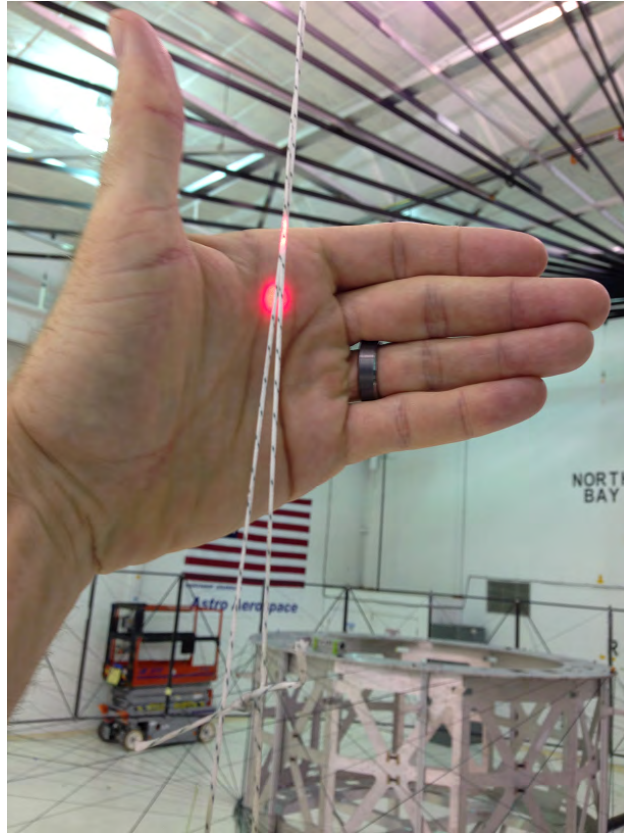


FIGURE 12. The intersection of the laser tracker beam, aimed at point OTR14, and a portion of the gravity compensation fixture.

- (2) The coordinate system of the model is chosen such that the center of the model coincides with the origin, and so the vectors between the measured and model points may be projected into radial (directly outward from origin) and tangential (perpendicular to radial) directions. Given this, we can constrain the alignment of the petal root points in a tangential direction. With a best-fit circle, as originally suggested in the white paper, no such constraints can be placed.

Figs. 13–17 show the spread of the laser-tracker positions over the 16 deployments. As we have a set of coordinate transformations which take each of the 16 sets of data into a coordinate system with the model center of the truss at the origin, we have transformed them into radial and tangential coordinates as well. Note these are deviations from each points mean only.

7.3. Analysis and application to milestone. The statistical tool we will use to check whether the milestone has been met is the tolerance interval(2). Unlike a confidence interval, which provides confidence bounds on the value of a parameter, a tolerance interval provides confidence bounds on a range of data. For our milestone, we wish to create a tolerance interval such that we are 90% confident it contains 99.73% of the population of future data points. (For a normal distribution, 99.73% of the distribution falls in the mean $\pm 3\sigma$.)

While the concept of a tolerance interval can be generalized to many distributions and use cases, for our purposes it takes the form

$$\bar{x} \pm ks \tag{1}$$

with \bar{x} is the sample mean and s the sample standard deviation. (We will assume these are derived from some n data points.) The primary difficulty lies in the calculation of k ; exact solutions can

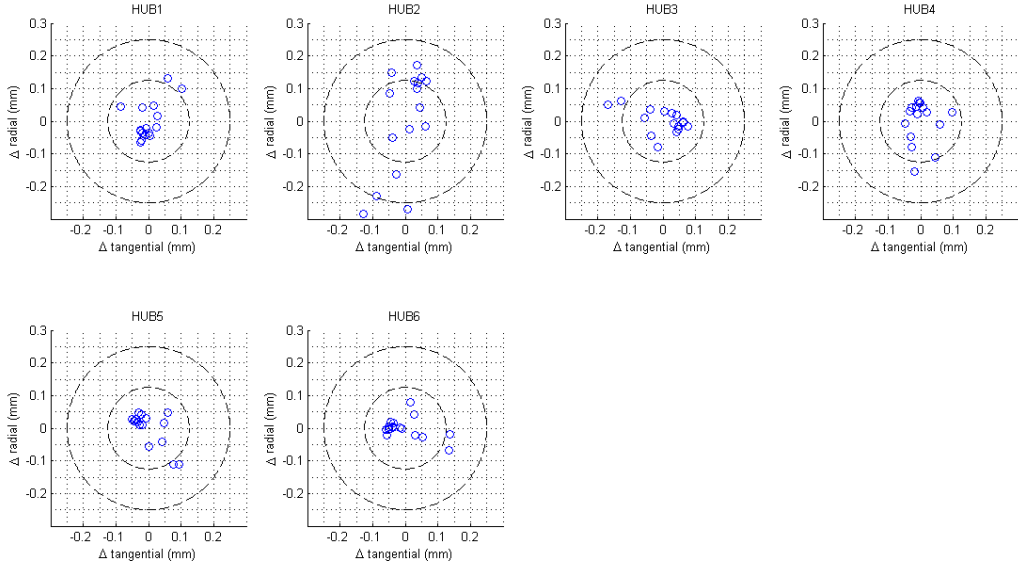


FIGURE 13. The spread of hub points over the 16 deployments. Radial and tangential directions are the (r, θ) unit vectors in a polar coordinate system with the nominal occulter center at the origin. Blue circles represent individual deployments. Circles of radius $125\mu\text{m}$ and $250\mu\text{m}$ are shown for scale.

TABLE 2. Tolerance intervals on displacement from model positions to contain 99.73% of population with 90% confidence

Point	Radial interval	Tangential interval
P1P	$[-0.075\text{mm}, 0.228\text{mm}]$	$[0.338\text{mm}, 0.479\text{mm}]$
P1S	$[-0.114\text{mm}, 0.153\text{mm}]$	$[0.232\text{mm}, 0.360\text{mm}]$
P2S	$[-0.102\text{mm}, 0.119\text{mm}]$	$[-0.088\text{mm}, 0.092\text{mm}]$
P2P	$[-0.091\text{mm}, 0.241\text{mm}]$	$[-0.082\text{mm}, -0.009\text{mm}]$
P3P	$[-0.011\text{mm}, 0.329\text{mm}]$	$[0.022\text{mm}, 0.125\text{mm}]$
P3S	$[-0.079\text{mm}, 0.271\text{mm}]$	$[-0.095\text{mm}, 0.036\text{mm}]$
P4S	$[-0.178\text{mm}, 0.151\text{mm}]$	$[-0.373\text{mm}, -0.212\text{mm}]$
P4P	$[-0.055\text{mm}, 0.165\text{mm}]$	$[-0.496\text{mm}, -0.327\text{mm}]$

be quite numerically involved, but there exist a number of widely-used approximations that for our data set will overestimate k by less than a percent (3). The approximation we chose, Eq. 9 in (3), gives:

$$k = \sqrt{\frac{(n-1)\chi_{1,\gamma}(1/n)}{\chi_{n-1,\alpha}}} \quad (2)$$

with $\chi_{n-1,\alpha}$ a quantile from a standard chi-square distribution and $\chi_{1,\gamma}(1/n)$ a quantile from a non-central chi-square distribution. (Quantiles from both distributions may be easily calculated in Matlab, which drove the selection of this approximation over others of comparable performance.)

For a 90% confidence ($1 - \alpha = 0.9$), $\gamma = 99.73\%$ of the data, and $n = 16$ data points, $k = 4.0897$. The resulting tolerance intervals are given graphically in Figure 18 and in tabular form in Table 2.

A primary assumption underlying the creation of tolerance intervals as above is the assumption of normality in the data, or at least being sufficiently close to normality that we don't invalidate the assumptions leading to the calculation of k . While approaches to interval creation exist without making assumptions on the underlying distribution of the data ("distribution-free"), these come

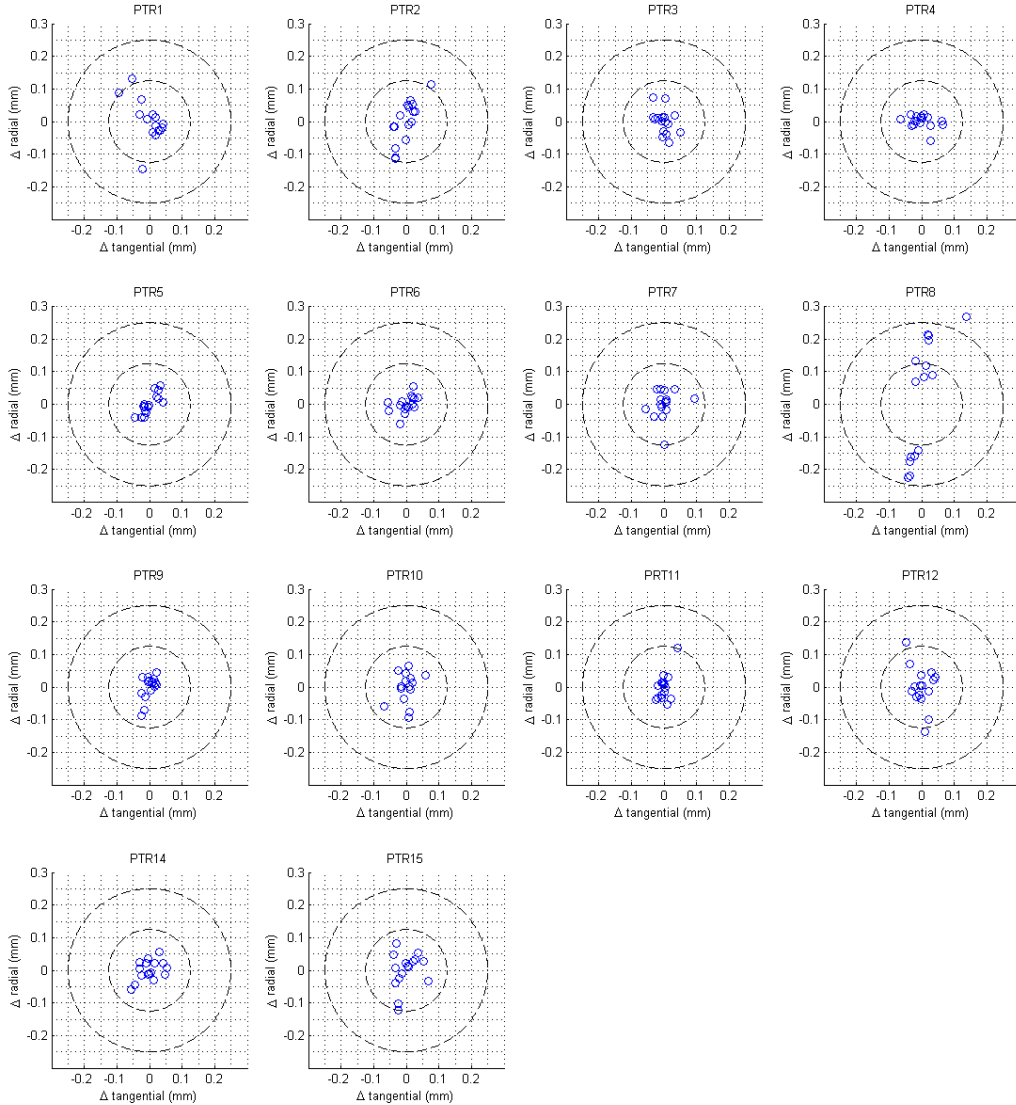


FIGURE 14. The spread of petal truss ring points over the 16 deployments. Radial and tangential directions are the (r, θ) unit vectors in a polar coordinate system with the nominal occulter center at the origin. Blue circles represent individual deployments. Circles of radius $125\mu\text{m}$ and $250\mu\text{m}$ are shown for scale.

with strong requirements on minimum sample size (2). Creating a distribution-free tolerance interval which contains 99.73% of future data points with 90% confidence requires a minimum of 1440 deployments to be completed, clearly an infeasible task given the cost and schedule constraints of this TDEM.

Figure 18 shows the mean deviation of the 8 petal root points after the 15 deployments with the resulting tolerance intervals, in both the radial and tangential directions, shown in blue. Radial errors show a small residual bias of 0.06 mm that could be reduced with additional shimming, though

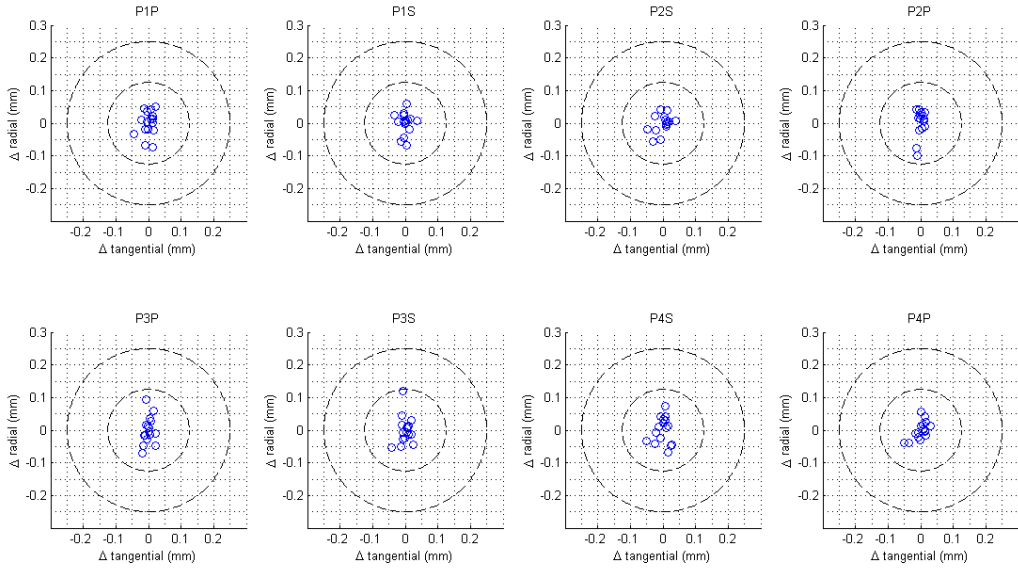


FIGURE 15. The spread of petal root points over the 16 deployments. Radial and tangential directions are the (r, θ) unit vectors in a polar coordinate system with the nominal occulter center at the origin. Blue circles represent individual deployments. Circles of radius $125\mu\text{m}$ and $250\mu\text{m}$ are shown for scale.

such a bias is still well within the error tolerance. The random tangential errors are minimal for the two inner petals and larger but still well within the tolerance limit for the two outer petals. This behavior is an expected manifestation of using existing hardware. The petals need to be registered to truss nodes (junction between bays) as they are the only points with precision deployment repeatability. The existing Astromesh antenna provides no registration features to precisely locate the nodal position. A retrofitted registration feature was possible for only the primary nodes, but not the alternating dependent nodes. A registration tool was installed to the primary node between petals 2 and 3 (attach points 4 and 5). A precision tool is used to locate attach points 3 and 6. Attach points on petals 1 and 2 (attach points 1, 2, 7 and 8) are positioned with further extrapolation and the errors start compounding. Future custom designs will include the necessary registration features at every node.

This figure illustrates that even at 90% confidence, we are well within the TDEM milestone requirement. In fact, if we rescale the performance (bias and random error) to the full size truss and insert into our error budget, we find that the 90% confidence contrast level is roughly 8×10^{-13} for the radial bias and 6×10^{-13} for the random radial and tangential performance. This is well within the allocated contrast level for these deployment errors in a flight system targeting 10^{-10} contrast.

8. CONCLUSIONS

This report shows that we successfully met our milestone of repeated deployments with ± 0.95 and 1.6 mm accuracy in the radial and tangential directions, respectively, corresponding to a 3σ contrast of 10^{-9} . In fact, we did better than this by a substantial margin, achieving an equivalent contrast of better than 10^{-12} due to deployment errors. A system with more control over the tangential position we would achieve an even better contrast. While the experiment employed a central truss that is not the same design as an eventual flight system and didn't allow the continuous

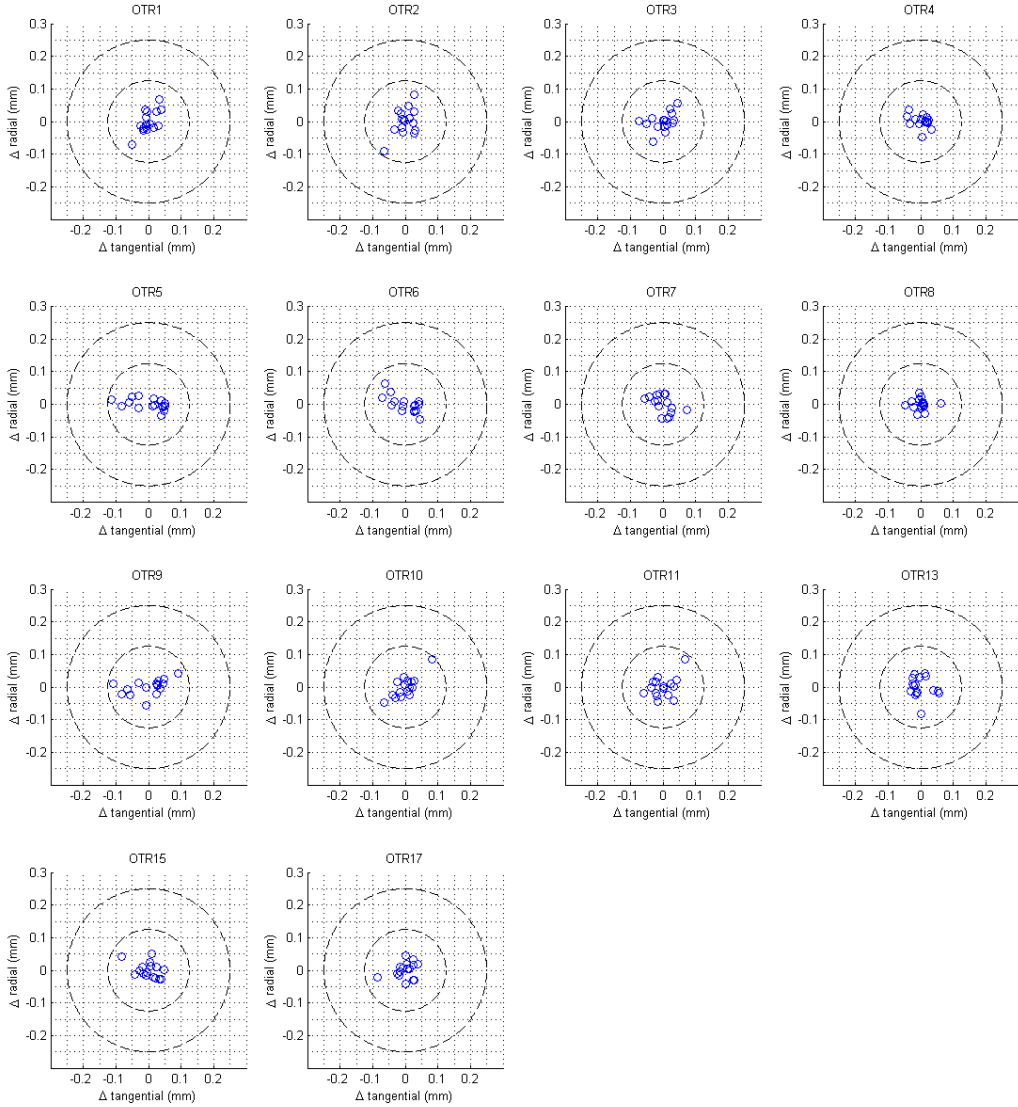


FIGURE 16. The spread of opposite truss ring points over the 16 deployments. Radial and tangential directions are the (r, θ) unit vectors in a polar coordinate system with the nominal occulter center at the origin. Blue circles represent individual deployments. Circles of radius $125\mu\text{m}$ and $250\mu\text{m}$ are shown for scale.

unfurling and deploying of the petals and starshade, it did demonstrate the feasibility of meeting the stringent deployment requirements with existing mechanical systems. This retires a major technology element of starshade manufacture.

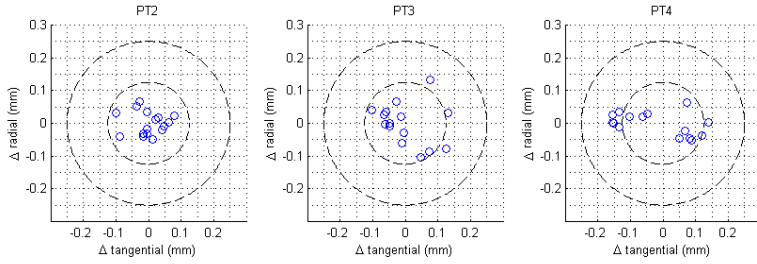


FIGURE 17. The spread of tip points over the 16 deployments. Radial and tangential directions are the (r, θ) unit vectors in a polar coordinate system with the nominal occulter center at the origin. Blue circles represent individual deployments. Circles of radius $125\mu\text{m}$ and $250\mu\text{m}$ are shown for scale.

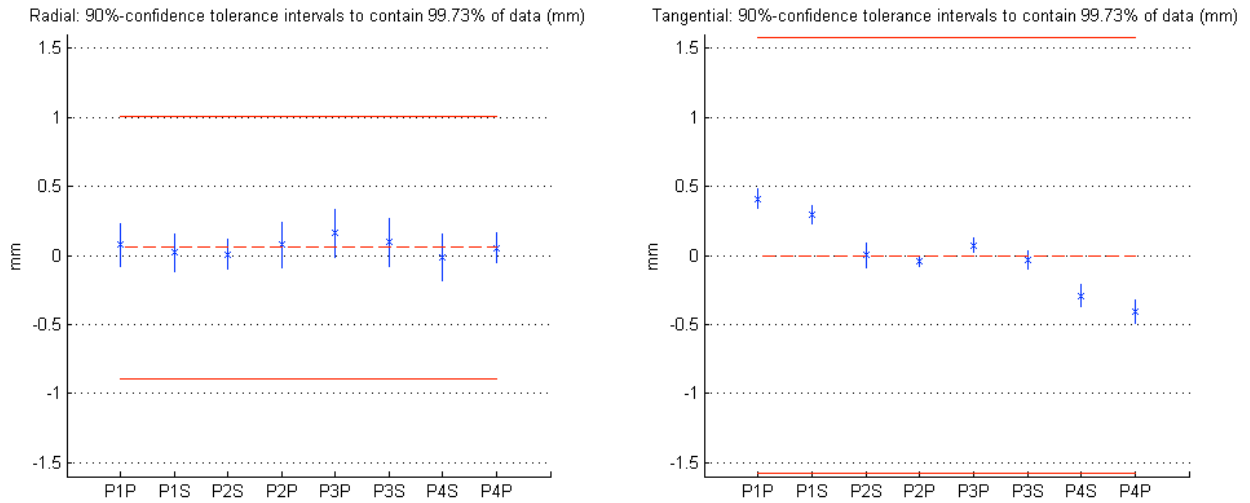


FIGURE 18. A set of tolerance intervals, shown in blue, for the eight petal root points which contain 99.73% of deployments with 90% confidence. *Left.* In the radial direction. *Right.* In the tangential direction. Red solid lines are the milestone required positioning errors and red dashed lines are the average biases of the radial and tangential deployments.

9. ACKNOWLEDGEMENT

This work was completed under a grant from the National Aeronautics and Space Administration (NASA), grant no. NNX12AD98G.

APPENDIX A. SUCCESS CRITERIA FROM WHITE PAPER

In TDEM-1, our success criterion was based on the ultimate contrast an occulter achieved. This had the advantage of being directly traceable to the requirements of an imaging mission. This criterion was established through a combination of metrology and modeling, using analysis of the measured data to make a prediction of the contrast from an occulter made from similar petals as that measured. This approach was sensible because of the large number of measurements made along the petal edges and the limitation of any error analysis that reduces those measurements to a small number of parametric terms. We thus came to a statistical estimate of the likely contrast.

In this second TDEM project, such an end-to-end analysis is not necessary. Here we have only a small number of measurements of three error parameters: the petal base point radial and transverse position and the petal rotation. These three error terms are directly traceable to contrast via the error budgeting process described in §2. A detailed conversion to contrast as we did in TDEM-1 would be superfluous and unnecessarily cumbersome. We therefore establish success through the process described above, repeatedly measuring the petal positions after deployment, combining the measurements, and comparing to the 3σ requirements. This process can be summarized as follows:

- (1) Mount petals on truss.
- (2) Deploy truss with attached petals using the gravity offload fixture.
- (3) Measure the base targets of each petal relative to the fixed fiducial origin.
- (4) Perform fit to find best fit circle to base positions.
- (5) Process measurements to determine radial and transverse bias of circle and radial and transverse positions of each petal as well as in plane rotation.
- (6) Repeat steps 1-5 n times. Process the n measurements as described §5 to determine best estimates of radial, transverse, and rotational errors with confidence intervals to determine if milestone requirement was met with 90% confidence.

APPENDIX B. TABLE OF ACRONYMS

Acronym	Meaning
CTE	Coefficient of Thermal Expansion
GCF	Gravity Compensation Fixture
GFRP	Graphite Fiber Reinforced Plastic
IWA	Inner Working Angle
JPL	Jet Propulsion Laboratory
NASA	National Aeronautics and Space Administration
POC	Proof of Concept
TDEM	Technology Development for Exoplanet Missions
THEIA	Telescope for Habitable Exoplanets and Intergalactic Astronomy
TRL	Technology Readiness Level

TABLE 3. A list of acronyms used in the report and their meanings.

REFERENCES

- [1] R. J. Vanderbei, E. J. Cady, and N. J. Kasdin. Optimal occulter design for finding extrasolar planets. *Astrophysical Journal*, 665:794–798, 2007.
- [2] G. J. Hahn and W. Q. Meeker. *Statistical Intervals: A Guide for Practitioners*. John Wiley and Sons, Inc., 1991.
- [3] W. A. Jensen. Approximations of tolerance intervals for normally distributed data. *Quality and Reliability Engineering International*, 25(5):571–580, 2009.
- [4] E. Cady. Boundary diffraction wave integrals for diffraction modeling of external occulters. *Optics Express*, 20:15196–15208, July 2012.
- [5] Stuart B. Shaklan, M. Charley Noecker, Tiffany Glassman, Amy S. Lo, Philip J. Dumont, N. Jeremy Kasdin, Eric J. Cady, Robert Vanderbei, and Peter R. Lawson. Error budgeting and tolerancing of starshades for exoplanet detection. volume 7731, page 77312G. SPIE, 2010.